



A damage-tolerant Ti-rich multiphase metallic-glass composite with hierarchically heterogeneous architecture

Shifeng Lin^{a,b,c}, Zhengwang Zhu^{a,b,c,*}, Zengqian Liu^{b,**}, Shaofan Ge^b, Dingming Liu^b, Hong Li^{a,b,c}, Zhengkun Li^{a,b,c}, Huameng Fu^{b,c}, Aimin Wang^{b,c}, Zhefeng Zhang^b, Haifeng Zhang^{a,b,c}, Robert O. Ritchie^{d,***}

^a School of Metallurgy, Northeastern University, Shenyang, 110819, China

^b Shi-changxu Innovation Center for Advanced Materials, Institute of Metal Research, Chinese Academy of Sciences, Shenyang, 110016, China

^c CAS Key Laboratory of Nuclear Materials and Safety Assessment, Institute of Metal Research, Chinese Academy of Sciences, Shenyang, 110016, China

^d Department of Materials Science and Engineering, University of California Berkeley, Berkeley, CA, 94720, USA

ARTICLE INFO

Handling Editor: Dr Hao Wang

Keywords:

Ti-Rich multiphase composite
Heterogeneity
Hierarchical structure
Mechanical properties
Toughening mechanisms

ABSTRACT

Lightweight materials with good combinations of properties, such as high strength, ductility and damage tolerance, are highly desirable in engineering applications; nevertheless, it remains a challenge to “defeat” the generally exclusive relationships between different properties for structural materials. One viable means is to construct complicated architectures in materials. Here, we employ a lightweight Ti-based metallic glass (MG) and pure Ti as constituents and assemble them into a hierarchically-structured multiphase composite with tailored heterogeneity. The Ti-rich multiphase composite exhibits a relatively low density of $4.95 \text{ g} \cdot \text{cm}^{-3}$ owing to its high Ti content and a high strength of $\sim 1408 \text{ MPa}$ derived primarily from the MG phase. The hierarchical architecture with tailored heterogeneity promotes the formation of abundant shear bands and microcracks in MG, yet inhibits their extension to avoid catastrophic fracture, thereby endowing the Ti-rich multiphase composite with a remarkable tensile ductility of $\sim 7.1\%$ which is nearly two times that of the MG composite having similar phase constitution but a uniform structure. Moreover, this architecture causes crack-tip blunting by promoting plastic deformation, together with crack bifurcation and microcracking ahead of the crack tip, which bestows a high (notched) fracture toughness of $\sim 109 \text{ MPa} \cdot \text{m}^{1/2}$ which is around three times that of its counterpart. This study is intended to give insight for the architectural design of new materials by offering a viable means for their architectural construction to achieve good combinations of properties.

1. Introduction

Light alloys with a good combination of multiple mechanical properties, such as high strength, ductility and fracture toughness, are highly desirable in a range of fields such as aerospace, automotive and energy transportation. Despite a lightweight and relatively low cost compared to other metallic alloys, the wide-spread proliferation of Mg alloys [1] and Al alloys [2,3] in structural applications can be compromised by their limitation in strength. Bulk metallic glasses (BMGs) are promising because they exhibit a high strength deriving from their amorphous structure, with the absence of any crystalline defects as their crystalline counterparts [4,5]. Among them, Ti-based BMGs which typically show a

high tensile fracture strength in excess of 1.5 GPa are attractive candidates for applications as high-strength materials [6,7]. Compared to Al alloys and Mg alloys, Ti-based BMGs with a high Ti content also exhibit a relatively low density (although their density is higher than that of Al- and Mg-alloys), but are more appealing owing to their higher strengths, higher hardness and larger elastic strain limit [6–8].

Unlike their crystalline counterparts, BMGs are free of grain boundaries, dislocations, or other crystalline defects and as such deform essentially through the highly localized shear bands [9–11]. As a result, BMGs are often brittle at room temperature, *i.e.*, the high strength of BMGs is generated at the expense of ductility, which limits their structural application. The brittle fracture of BMGs is closely related to their

* Corresponding author. School of Metallurgy, Northeastern University, Shenyang, 110819, China.

** Corresponding author.

*** Corresponding author.

E-mail addresses: zwzhu@imr.ac.cn (Z. Zhu), zengqianliu@imr.ac.cn (Z. Liu), roritchie@lbl.gov (R.O. Ritchie).

unique mechanisms of plastic deformation which is mediated via narrow shear bands [4,11]. Accordingly, interrupting the propagation of shear bands is the key for generating ductility in BMGs. The incorporation of a second phase (or multiple phases) into the BMG matrix to construct composite structure offers an effective means to this end [5,8,12–19]. This can be realized either by *in situ* precipitation of a second phase from the metallic melts during solidification [8,12–16], or by artificially assembling the matrix material with the second phase via *ex situ* methods [17–19]. The shear bands in the resultant bulk metallic glass composites (BMGCs) can be spatially confined by the second phase upon loading; this can trigger the formation of an increased number of shear bands to confer ductility to BMGCs. Generally, reasonable tensile ductility is more easily accessible in the *in situ* BMGCs due to their strong interfacial bonding between the toughening phases and the BMG matrix; however, this is rarely attainable in the *ex situ* BMGCs [5,18,19]. Nevertheless, the microstructural characteristics of BMGCs can be more easily modulated by *ex situ* methods for tailoring their mechanical properties, which is not so easy to realize in *in situ* BMGCs.

The attainment of tensile ductility in BMGCs is often accompanied by a compromise in strength compared to the BMG matrix. The early developed *in situ* BMGCs [8,12,13] usually displayed macroscopic strain softening behavior under tension which leads to an instability in the form of unstable necking upon yielding. Inspired by the martensitic transformation-induced work-hardening behavior in steels [20], Ti alloys [21,22] and B2–CuZr alloys [23], a series of *in situ* BMGCs toughened by metastable crystals have been successfully developed by accurately modulating the concentration of the β or B2–CuZr phase stabilizers [14,16,24]. This approach serves to delay the onset of inhomogeneous deformation, which enhances the uniform ductility, although these BMGCs often exhibit a marked decrease in strength, especially the yield strength, because the deformation-induced martensitic phase transformation occurs at a relatively low stress level. To date, such a tradeoff has only been overcome in a limited number of Zr-based BMGCs; however, these materials are not lightweight as they primarily consist of heavy elements and thus possess a high density [8,15].

In addition to strength and ductility, the fracture toughness, which describes the resistance to the initiation and propagation of cracks, is another key property of structural materials. For BMGs and BMGCs, it has been a challenge to achieve a good combination of strength, tensile ductility and fracture toughness in a single material. Some Pd-rich and Zr-based BMGs show high strength of 1.5–1.6 GPa and high fracture toughness of 100–200 MPa m^{1/2}, yet display near-zero tensile ductility [10,25–27]. Zr-based BMGC (with a composition of Zr_{39.6}Ti_{33.9}Nb_{7.6}Cu_{4.66}Be_{12.5}, at.%) shows a high fracture toughness of ~173 MPa m^{1/2} and good tensile ductility of 13.1% while concomitantly preserving a high yield strength of 1096 MPa and an ultimate tensile strength of 1210 MPa [12,28,29]. However, this Zr-based BMGC has a high density which degrades its weight-normalized (specific) properties. For the lightweight Ti-based BMGCs (with Ti content higher than 50 at.%), although a good combination of strength and tensile ductility can be achieved by adding the element V, they still exhibit limited fracture toughness not exceeding 65 MPa m^{1/2} [8]. Accordingly, the objective of the current work is to enhance the ductility and damage tolerance while retaining a high strength in lightweight Ti-rich composite materials based on Ti-based BMGs.

Natural materials, such as nacre, wood and bone, are composed of relatively hard and soft phases which are arranged in complex hierarchical architectures with large heterogeneity - structures that have been proven to be effective in generating remarkable damage tolerance [30–32]. Consequently, these natural materials have been widely mimicked by implementing their underlying design principles into a range of synthetic materials with enhanced mechanical properties [33–35]. Here we exploit a new lightweight Ti-rich composite composed of metallic glass (MG), α -Ti and β -Ti phases by intentionally constructing a hierarchical structure with tailored heterogeneity. Such an

architecture confers the composite with high damage tolerance in the form of an excellent combination of high strength, uniform tensile ductility and fracture toughness. We also elucidate the salient mechanisms associated with the formation, deformation and toughening effects in the Ti-rich multiphase composite, which we believe will afford new insights for the generation of new damage-tolerant materials.

2. Experimental

2.1. Fabrication of MG and Ti ribbons

An alloy ingot with nominal composition of Ti_{31.16}Zr_{28.69}Ni_{5.04}Cu_{8.55}Be_{21.56}Mo₅ (at.%) was prepared by arc melting the mixture of constituents under Ti-gettered high purity argon atmosphere. The alloy ingot was repeatedly melted by at least four times to ensure the chemical homogeneity. Metallic glass ribbons, ~50 μ m in thickness and ~10 mm in width, were produced using a melt spinning method by injecting the alloy melt onto a copper roller rotating at 1800 m/min. Subsequently, the MG ribbons were cut into sections 80 mm in length. Commercial pure Ti foils (50 μ m in thickness) of fully hexagonal close-packed (*hcp*) structured α -Ti phase (with purity >99.9 wt%) were cut to the same dimensions as the MG ribbons, prior to being ultrasonically cleaned in ethanol.

2.2. Fabrication of Ti-rich multiphase composite

The ribbons of MG and pure Ti were stacked alternately in a holding fixture and then closely compacted. The preform, with a thickness of 9 mm, was then sealed into a vacuumed square tube of stainless steel. To fabricate the Ti-rich multiphase composite, this tube was placed in a furnace for 2 min at 895 °C (*i.e.*, ~105 °C higher than the melting temperature of the MG) and then quenched into water (Fig. S1 in Supplementary Materials). For comparison, an *in situ* BMGC, where β -Ti dendrites were precipitated from the MG matrix, was also prepared (in dimensions of 60 × 12 × 6 mm³) using a copper mold tilt casting technique [16,24]. This material had a similar Ti_{63.17}Zr_{15.65}Ni_{2.75}Cu_{4.66}Be_{11.77}Mo₂ (at.%) composition as the Ti-rich multiphase composite (*i.e.*, by incorporating the Ti ribbons, the composition of the multiphase composite approximates to that of the *in situ* BMGC), but exhibited a uniform composite architecture with the β -Ti dendrites being homogeneously distributed in the MG matrix.

2.3. Characterization of the phase constitutions and microstructures

The phase constitutions of the Ti-rich multiphase composite were characterized by means of X-ray diffraction (XRD, Philips PW1050, Cu-K α), differential scanning calorimetry (DSC, Netzsch 204F1) and transmission electron microscopy (TEM, FEI Tecnai F20). The microstructures of this material before and after deformation were observed by scanning electron microscopy (SEM, Zeiss Supra 55) combined with energy-dispersive X-ray spectroscopy (EDS, Oxford). For the TEM observations, specimens (cut from the as-cast sample) with a diameter of 3 mm were mechanically ground to a thickness of 45 μ m, dimpled to reduce the central thickness to about 10 μ m, and then ion-milled using a Gatan 691 device with liquid nitrogen cooling.

2.4. Mechanical testing

Tensile samples were made in a dog-bone plate shape with a gauge dimension of 15 mm (length) × 2.5 mm (width) × 1 mm (thickness). Uniaxial tension tests were conducted on an Instron 5582 universal testing machine at an initial strain rate of 0.1 mm/min with the strain measured using an extensometer mounted on the specimen. Samples for unnotched and single-edge notched bending SE(B) tests were cut to dimensions of 30 mm (length, *L*) × 5 mm (width, *W*) × 2.5 mm (thickness, *B*). Notches with a root diameter of ~125 μ m were cut to a depth of

0.45–0.55W for the fracture toughness tests on the SE(B) specimens of the BMGCs. Both unnotched and SE(B) specimens were tested on an Instron 5582 testing machine in three-point bending with a loading span distance (S) of 20 mm and a displacement rate of 0.1 mm/min. At least three samples were tested for each microstructural condition for each type of mechanical test. The detailed procedure of fracture toughness determination was seen in the Supplementary Materials. Nano-indentation measurements were also performed on carefully polished and etched samples using an Agilent, G200 nanoindenter, operated in the continuous stiffness mode at a displacement rate of 10 nm/s to indentation depths of 500 nm.

3. Results and discussion

3.1. Microstructural characteristics

As shown in Fig. 1(a and b) and Fig. S1 in the Supplementary Material, the resulting Ti-rich multiphase composite displays a layered architecture with different constituents alternately arranged. The interfaces between the metallic glass and Ti layers can be seen to be highly tortuous, with coarse dendrites distributed within the MG layers. X-ray diffraction (XRD) patterns show that the peaks of the crystalline phases from both the α - and β -Ti phases are superimposed on the broad diffuse scattering of the MG phase (Fig. S2(a)), indicating that the Ti-rich composite is composed of α -Ti, β -Ti and MG phases. The presence of the MG phase can be additionally confirmed by differential scanning calorimetry (DSC) which clearly reveals characteristic glass transition behavior and a supercooled liquid region (Fig. S2(b)). By analyzing scanning electron microscopy (SEM) images, the volume fractions

(Table S1) of the α -Ti, β -Ti and MG phases were estimated to be 16.3–20.0%, 39.1–42.8%, and 39.3–43.1%, respectively. Transmission electron microscopy (TEM) revealed that the crystalline Ti layer in the Ti-rich multiphase composite principally consists of the outer β -Ti and inner α -Ti phases (Fig. 1(c)). The inner α -Ti phase additionally exhibits a gradient structure with the grain size increasing towards the interior of the Ti layer (Fig. S3 and Fig. 1(c-e)), which ranges hundreds of nanometers to micrometers. By comparison, the structure of the as cast *in situ* BMGC with similar composition as the multiphase composite is characterized by a uniform distribution of β -Ti dendrites which account for a volume fraction of $65.3 \pm 2\%$ in the MG matrix, as shown in Fig. S4.

The fabrication approach used for the current multiphase composite is to some extent similar to a metal welding process where MG melts are used to bond the adjacent Ti layers. Metal welding has been previously reported to often lead to the formation of detrimental intermetallic compounds or voids at the interfaces in *ex situ* BMGCs [18,19] or in composites comprising MG as a compliant phase [17]. However, these defects were not found in the current composite, implying a good interfacial bonding between the Ti and MG layers, as shown in Fig. 1(b). It is considered that the good wettability and compatibility between the Ti layers and the selected MG melt led to a strong liquid/solid interaction in the preparation process to form thermodynamically stable dendrites instead of brittle intermetallic compounds at their interfaces. Additionally, the formation of voids can be inhibited by the employment of high vacuum condition during processing. The Ti/MG interfaces in our Ti-rich multiphase composite additionally feature a microscopically zig-zag trajectory, with the α -Ti layers, which are originally $\sim 50 \mu\text{m}$ in thickness, becoming thinner. In general, the precipitated crystalline phases are known to be homogeneously distributed within the MG

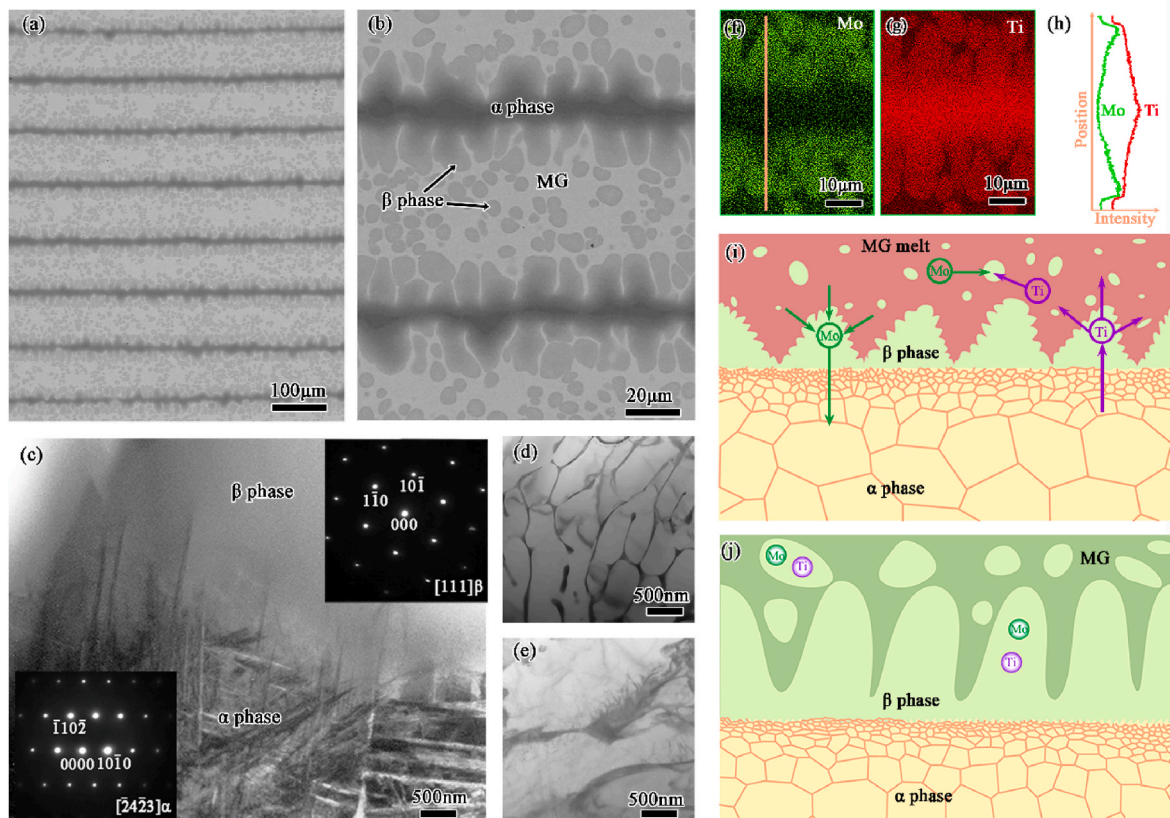


Fig. 1. Microstructure of the Ti-rich multiphase composite. (a, b) SEM images of the Ti-rich multiphase composite. TEM micrographs of (c) the interfacial region between the β -Ti dendrite and α -Ti layer and of the (d) exterior to (e) interior of the α -Ti layer. The insets in (c) show the selected area electron diffraction (SAED) patterns of the α -Ti and β -Ti phases. Area distribution of (f) Mo and (g) Ti elements and (h) their linear distribution through the α -Ti layer along the yellow line. Schematic illustration of the formation mechanism of architecture in the Ti-rich multiphase composite with the architectural evolution (i) at high temperature and (j) after quenching. (For interpretation of the references to colour in this figure legend, the reader is referred to the Web version of this article.)

matrix in a dendritic form (with fine dendrite arms and different dendrite spacings) in similar materials, such as, for example, Ti/Zr-based *in situ* BMGCs (Fig. S4) [8,12,14,24]. By contrast, a large number of nearly elliptical-shaped precipitates of the β -Ti phase with a diameter of 2–20 μm are formed in the MG matrix for the current composite.

The compositions of the precipitated dendrites and MG matrix in the Ti-rich multiphase composite were determined to be respectively $\text{Ti}_{75.4}\text{Zr}_{13.6}\text{Ni}_{0.8}\text{Cu}_2\text{Mo}_{8.2}$ and $\text{Ti}_{53.1}\text{Zr}_{30.4}\text{Ni}_{6.4}\text{Cu}_{10.2}$ (at.%) using energy-dispersive x-ray spectroscopy (EDS) (Note that the Be content cannot be precisely quantified using EDS, but this element has been revealed to be principally dissolved in the MG matrix [8,12], otherwise the BCC crystalline structure of dendrites will be severely distorted due to the large mismatch of atomic radii when a small amount of Be is dissolved in β -Ti phase). Mo, which was originally contained in the MG layers, was clearly expelled from the MG matrix into the β -Ti phase (Fig. 1(f, h)). This is caused by the fact that Mo is a strong β -stabilizing element and has a limited solubility in the MG matrix [24]. Additionally, the contents of Mo and Ti elements are nearly identical in the β -Ti phases extended from the Ti layer and in the dendrites distributed in the MG matrix. EDS results further revealed a gradient distribution of the two elements in the α -Ti phase (Fig. 1(f–h)), with a decrease in the Mo content from the exterior to interior but with an opposite variation for the Ti element. It is worth noting that the Zr, Ni and Cu elements show a similar gradient change as the Mo element in the crystalline layer (Fig. S1). Such gradients in chemical composition are accompanied by an increase in the grain size of the α -Ti phase (Fig. 1(c–e)).

The formation mechanism of the Ti-rich multiphase composite, which involves a strong liquid/solid interaction with the dissolution and diffusion of elements at high temperatures, is schematically illustrated in Fig. 1(i and j). During the liquid/solid interaction, the Ti atoms diffuse from the Ti layer into the melt while the Mo atoms diffuse in the opposite direction. The Mo element has a positive mixing enthalpy with the other elements in the MG melt [37], and plays a central role in stabilizing the β -Ti phase in generating the multiphase composite architecture. The redistribution of elements eventually leads to the accumulation of Mo in the β -Ti dendrites, either extending from the α -Ti layer or distributed in the MG matrix. Additionally, the diffusion of Mo into Ti layer induces a lattice transition from α -Ti to β -Ti with the grain refinement of the α -Ti phase. The Mo atoms, combined with the Ti atoms diffused from the Ti

layer, form thermodynamically-stable β -Ti crystals which grow into the *in situ* dendrites in the MG matrix during subsequent cooling. The exfoliation of the β -Ti dendrites from the Ti layer also acts as nucleation sites for the *in situ* dendrites. Additionally, the β -Ti dendrites transformed from the α -Ti phase extend from the α -Ti layer into the MG matrix. In this process, the thickness of the α -Ti layer decreases continuously with the growth of the β -Ti dendrites. The Mo in solid solution also induces the grain refinement of the α -Ti phase. As such, the α -Ti layer exhibits a gradient nature in both chemical composition and structure, *i.e.*, with a decrease in Mo content and an increase in Ti content with a progressive enlargement in the grain size from the exterior to interior locations. The extension of β -Ti dendrites into the MG matrix from the α -Ti layer additionally leads to the zig-zag interface between the constituent layers.

3.2. Mechanical properties

Unlike the *in situ* BMGC with uniform composite architecture where the stress decreases after yielding, the Ti-rich multiphase composite exhibits apparent work-hardening ability to achieve high yield and ultimate tensile strengths of, respectively, ~ 1221 MPa and ~ 1408 MPa (Fig. 2(a)). These values are slightly lower than those of the *in situ* homogeneous BMGC where both the yield and ultimate strengths were measured as ~ 1492 MPa. However, the tensile elongation is increased by more than two-fold, from $\sim 3.1\%$ for the *in situ* homogeneous BMGC to $\sim 7.1\%$ for the Ti-rich multiphase composite. Moreover, the uniform elongation of the Ti-rich multiphase composite markedly outperforms that of the *in situ* homogeneous BMGC. Such a combination of high strength with good ductility has rarely been obtained in MG-containing composites [18,19]. Additionally, the mechanical properties of the Ti-rich multiphase composite are far superior to the *in situ* homogeneous BMGC under three-point bending conditions (Fig. 2(b)). It shows a high flexural strength of ~ 2717 MPa and flexural plasticity of $\sim 10.3\%$. In comparison, the *in situ* homogeneous BMGC fails at a markedly lower flexural stress of ~ 1860 MPa and does not show any visible plasticity.

The difference in mechanical properties between the two materials results from their distinctly different composite architectures. Cracks are formed in the MG phase of the Ti-rich multiphase composite (inset in Fig. 2(b)); nevertheless, they are quite stable and remain strictly confined within an individual MG layer without penetrating through the

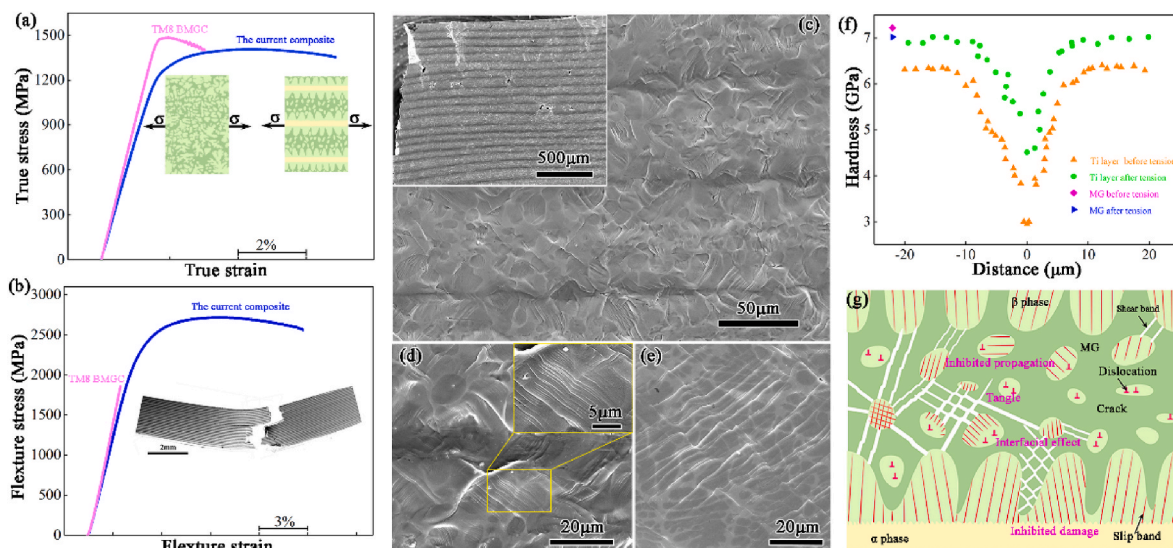


Fig. 2. Mechanical properties and deformation mechanisms of the Ti-rich multiphase composite. (a) Tensile and (b) flexural stress-strain curves of the Ti-rich multiphase composite compared to the *in situ* homogeneous BMGC. SEM images of the fractured samples of (c, d) the current composite and (e) the *in situ* homogeneous BMGC. (f) Profile of the hardness of the MG phase and across the Ti layer in the current Ti-rich multiphase composite before and after fracture. (g) Schematic illustration of the deformation and damage mechanisms in the Ti-rich multiphase composite showing the effects of the material's architecture.

ductile Ti layers into neighboring MG layers. A high stress is essentially needed for triggering the formation of these cracks due to an intrinsically high strength of the MG phase. Accordingly, the stable cracking effectively consumes a large amount of mechanical energy and enables extensive plastic deformation of the Ti-rich multiphase composite prior to final fracture, which is similar to the effect of tunnel cracks observed in many laminated composites [36]. However, similar cracking processes are not present in the *in situ* homogeneous BMGC, implying a limited effect of the uniform composite architecture in confining crack extension.

The crystalline phases, *i.e.*, the ductile Ti layers and β -Ti dendrites, in the Ti-rich multiphase composite can also inhibit the propagation of primary shear bands in MG phase to promote their multiplication (Fig. 2 (c–e)). The straight extension of shear bands is distorted by the crystals, delaying the cavitation of shear bands to form cracks; this significantly contributes to the large ductility of the alloy. By comparison, a number of primary shear bands without visible proliferation of smaller ones are seen to penetrate through the *in situ* dendrites in the *in situ* homogeneous BMGC, with the result that the shear bands easily evolve into unstable cracks due to the lack of formidable barriers to inhibit crack extension. However, under three-point bending conditions, the heterogeneous architecture of the Ti-rich multiphase composite markedly promotes the proliferation of shear bands which is the primary source of plasticity in BMGs (Fig. S5). Conversely, the uniform composite architecture cannot actuate the formation of visible shear bands, resulting in the limited-to-zero flexural ductility of the *in situ* homogeneous BMGC.

The proliferation of shear bands essentially leads to the softening of the MG phase in the Ti-rich multiphase composite, as evidenced by the decrease of hardness from ~ 7.22 GPa before tension to ~ 7.02 GPa after tension (Fig. 2(f)). The uniform deformation of the Ti-rich multiphase composite is associated with the plastic deformation and work-hardening behavior of the crystalline phase, especially of the ductile Ti layers (Fig. 2(c)), which acts to counter this softening. The volume fraction of crystals (consisting of β -Ti and α -Ti phases) in the Ti-rich multiphase composite is similar with that for the *in situ* homogeneous BMGC (Table S1 in the Supplementary Material); additionally, the α -Ti phase in the Ti-rich multiphase composite is intrinsically softer than the β -Ti and MG phases. Nevertheless, the α -Ti layer undergoes severe work-hardening during deformation (Fig. 2(f)), which is beneficial for enhancing the uniform plastic deformation of the Ti-rich multiphase composite. The gradient compositional and structural characteristics of the α -Ti layer induce a visible gradient in the hardness along it, both before and after deformation (Fig. 2(f)). It clearly shows that the hardness increases by ~ 1.56 GPa in the center of the α -Ti layer, and ~ 0.68 GPa from near the MG matrix to the interface between the α -Ti layer and the β -Ti layer after deformation. Akin to many natural materials, such gradients can result in unusual combinations of properties, in the present composite to a simultaneous enhancement in strength and ductility by creating extra strain hardening behavior through the conversion of an applied uniaxial stress into a multiaxial stress-state [38,39]. Additionally, the gradient structure effectively decreases the mechanical incompatibility between the pure α -Ti and β -Ti phases, thereby promoting effective stress transfer to prevent interfacial cracking between them. The relatively stronger β -Ti dendrites, compared to the α -Ti phase, can clearly also be work-hardened to counteract the strain softening in the MG phase.

The “Molybdenum equivalent” ($[Mo]_{eq}$) with an expression of $[Mo]_{eq} = 1.0[Mo] + 2.46[Ni] + 0.47[Zr] + 15.1[Cu]$ (wt.%) is a frequently used indicator for evaluating the stability of the β -Ti phase [40]. This parameter was calculated to be respectively 16.1% and 9.8% for the β -Ti phase in the Ti-rich multiphase composite and in the *in situ* homogeneous BMGC. Accordingly, it is evident that the β -Ti phase shows a higher stability in the Ti-rich multiphase composite than in the *in situ* homogeneous BMGC, along with a stonger plastic deformation capacity [16]. Additionally, the hardening effect of the β -Ti phase is limited, due to its fine dendrite arms, to counteract any work softening of the MG in

the *in situ* homogeneous BMGC (Fig. 2(e)) [13]. In comparison, the much coarser β -Ti dendrites, especially those extending from the Ti layers, in the Ti-rich multiphase composite not only arrest the propagation of shear bands in the MG phase but also generate a notable source of plastic deformation, as illustrated in Fig. 2(g).

The zig-zag interfaces between MG and Ti layers are beneficial for enhancing the interfacial toughness in the Ti-rich multiphase composite by increasing the interfacial area and by deflecting the extension of any interfacial cracks (Fig. 2(g)) [41,42]. Additionally, narrow grooves containing MG phase are created near the interfaces between the β -Ti dendrites, which actually can constrain the shear bands formed in the MG phase within the grooves (Fig. 2(g)) [4,43]. Moreover, the rough interfaces can readily induce shear bands directed at differing directions to enhance their mutual intersection.

3.3. Fracture toughness

To measure the fracture toughness of these materials, sharply-notched single edge-notched bend samples were used. A load-displacement curve from the SE(B) tests on the Ti-rich multiphase composite tested in three-point bending does not display simple linear-elastic fracture behavior, but rather encompasses several serration events (Fig. 3(a)), which delineate the occurrence of plastic deformation during crack growth. The fracture toughness of the Ti-rich multiphase composite was measured to be ~ 109 MPa m^{1/2}, which is a little higher to an as cast Ti-based BMG with fracture toughness of 102 MPa m^{1/2} [44]. The fracture surface shows crack deflection, crack branching and crack blunting characteristics (Fig. 3(b)), implying stable crack extension. In contrast, the reference *in situ* homogeneous BMGC fractures catastrophically with little evidence of gross plastic deformation, yielding a fracture toughness K_{Ic} of ~ 43 MPa m^{1/2}, *i.e.*, approximately 61% lower than that for the Ti-rich multiphase composite. The corresponding crack path is linear and straight without visible deflection (Fig. 3(c)).

The composition of the MG phase in the Ti-rich multiphase composite is similar with that of a previously reported Ti-based BMG [6] which possesses a high fracture toughness owing to a relatively high Poisson’s ratio of ~ 0.36 . However, the *in situ* homogeneous BMGC with similar composition as the Ti-rich multiphase composite demonstrates much poorer damage tolerance. As a result, we can conclude that the MG phase in the Ti-rich multiphase composite mainly contributes to the high strength, whereas the fracture toughness is principally derived from the heterogeneous composite architecture.

The arrest of shear bands by the crystalline Ti layers and β -Ti dendrites embedded in the MG phase promotes shear band multiplication to relieve local stress concentrations (Fig. 3(d and e)). This is definitively beneficial in preventing premature cavitation and cracking of the MG phase. In particular, the relatively soft α -Ti layer with a gradient in grain size dissipates mechanical energy to inhibit the propagation of the shear bands. However, such an effect is not active in the *in situ* homogeneous BMGC with a uniform composite architecture (Fig. 3(f)). Cavitation of the shear bands leads to the formation of cracks which can readily penetrate across the whole sample, leading to a limited fracture toughness compared to the Ti-rich multiphase composite.

The strong interface between the Ti and MG layers allows the Ti-rich multiphase composite to undergo large plastic deformation without interfacial cracking; its heterogeneous architecture consequently can result in a large plastic zone surrounding the crack tip (Fig. 3(d, g)), where apparent plastic deformation occurs to dissipative energy and blunt cracks. Further, the ductile Ti layer plays an effective role in confining these cracks. In particular, the gradient structure of the α -Ti layer is beneficial for blunting crack tips because the strain-hardening capability can be enhanced by the gradient as the cracks permeate into the ductile α -Ti layer along the gradient direction [45].

A number of microcracks emerge ahead of the crack tip in the Ti-rich multiphase composite (Fig. 3(d)), but are absent in the reference *in situ*

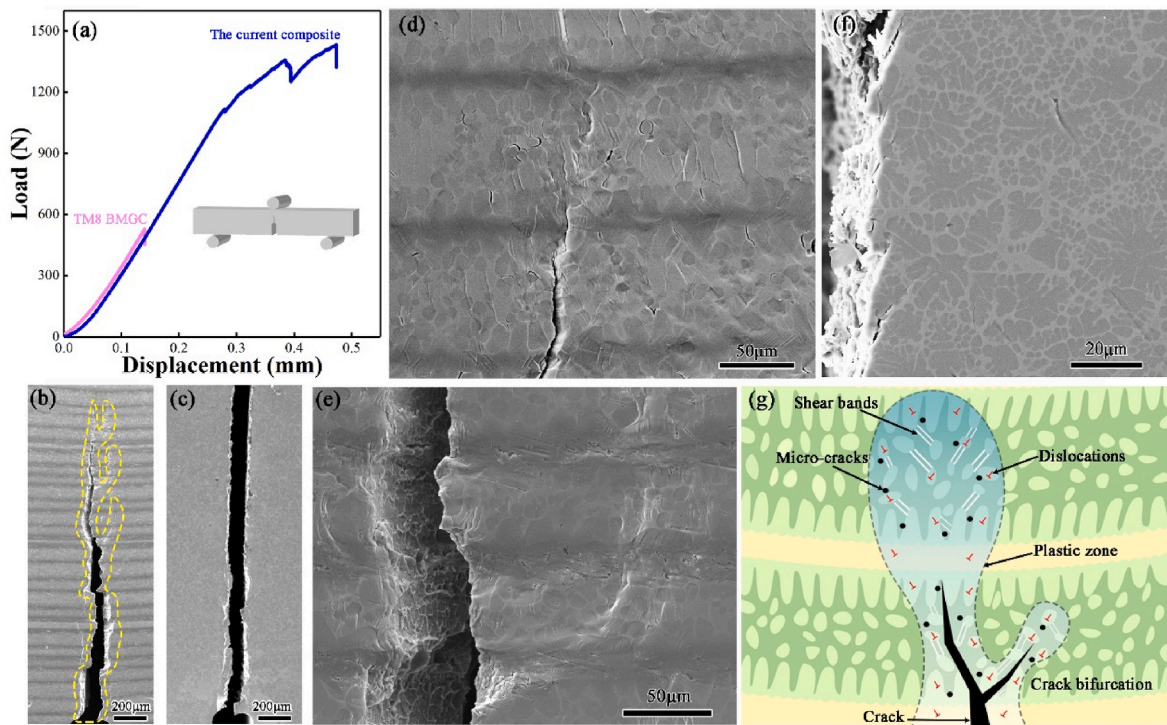


Fig. 3. Fracture toughness and toughening mechanisms of the Ti-rich multiphase composite compared to the *in situ* homogeneous BMGC. (a) Load-displacement curves of the Ti-rich multiphase composite and the *in situ* homogeneous BMGC under single-edge notched three-point bending conditions. SEM micrographs of the fracture surfaces of (b) the Ti-rich multiphase composite and (c) the *in situ* homogeneous BMGC. Micrographs of the regions (d) ahead of the crack tip and (e) near the cracking path in the Ti-rich multiphase composite. (f) Surface morphology of the *in situ* homogeneous BMGC after fracture. (g) Schematic illustration of the toughening mechanisms for the Ti-rich multiphase composite. (In (b) to (g), the crack is propagating from the bottom to the top of the page).

homogeneous BMGC with uniform composite architecture. These microcracks evolve from the shear bands induced by locally high stress concentrations, *e.g.*, at the interfaces between the β -Ti dendrites and MG phase. Such constrained microcracking can serve as a mechanism of inelasticity and thereby act to alleviate stress concentrations and release mechanical energy at the tip of main crack; this additionally contributes to toughening by retarding its crack growth [32,46].

The heterogeneous architecture and the elastic mismatch between different constituents also play a role in deflecting cracks in the Ti-rich multiphase composite (Fig. 3(b)). The hierarchically heterogeneous architecture can lead to a heterogeneous distribution of stress ahead of the crack tip to deflect the cracking path. In particular, the gradient Ti layer may induce any incipient cracks to continually change their propagation direction owing to the graded variation in elastic modulus across the

thickness [12]. Such crack deflection, as an extrinsic toughening mechanism [35], can further enhance the crack growth resistance by deviating the trajectory of any cracks from the path of maximum tensile stress; as a result, a higher stress is required to drive the advance of these cracks compared to the case for straight cracking path. Crack bifurcation was also observed in the Ti-rich multiphase composite (Fig. 3(b) and Fig. S6), which can aid the delocalization of damage, thereby promoting fracture resistance. In comparison, the primary crack in the *in situ* homogeneous BMGC was observed to be more prone to penetrating through the dendrites, leading to the catastrophic fracture of the entire sample.

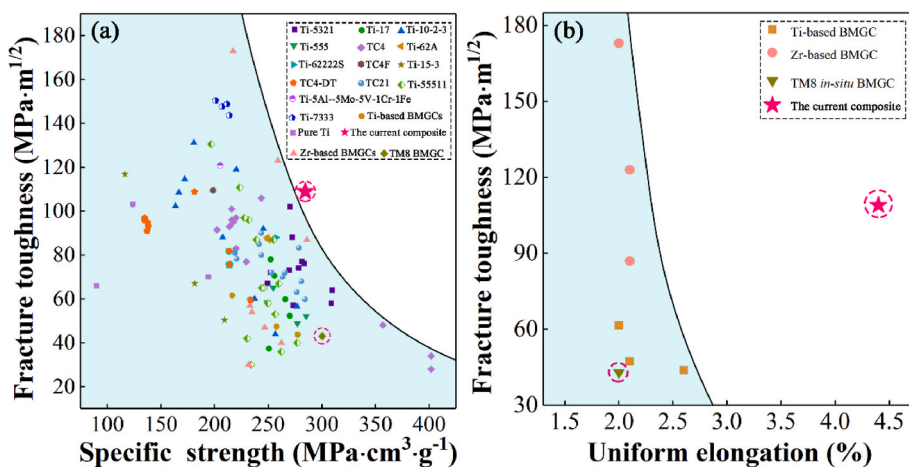


Fig. 4. Comparison of the mechanical properties of the current Ti-rich multiphase composite with other Ti alloys and BMGCs. (a) Fracture toughness versus specific strength. (b) Fracture toughness versus uniform tensile elongation (Ti-5321 [47,48], Ti-17 [49, 50], Ti-10-2-3 [49,51], Ti-555 [49], TC4 [52-54], Ti-62 A [55], Ti-62222S [55], TC4F [52], Ti-15-3 [56], TC4-DT [57,58], TC21 [59-61], Ti-55511 [62], Ti-5Al-5Mo-5V-1Cr-1Fe [63], Ti-7333 [64], Pure-Ti [8,65]). and BMGCs (Ti-based BMGCs [8], Zr-based BMGCs [12]).

3.4. Comparison with other materials

It is pertinent to compare the mechanical properties, *i.e.*, strength normalized by density (or specific strength), tensile ductility and fracture toughness, of our Ti-rich multiphase composite with a hierarchically heterogeneous architecture to those of other Ti alloys [47–65] and BMGCs [8,12] (Fig. 4). In this regard, the density of materials is a major consideration for structural applications. The current composite exhibits a relatively low density of $4.95 \text{ g} \cdot \text{cm}^{-3}$ as a result of its high Ti content; this density is qualitatively comparable to those of most Ti alloys. However, the strength of the Ti-rich multiphase composite outperforms that of the majority of other Ti alloys and Ti-based BMGCs [5, 8,40,47–65]. Additionally, the heterogeneous architecture of our Ti-rich multiphase composite generates a high fracture toughness of $\sim 109 \text{ MPa} \cdot \text{m}^{1/2}$. As shown in Fig. 4(a), the Ti-rich multiphase composite achieves a good combination of fracture toughness and specific strength among various Ti alloy and BMGC systems. It is noted that the fracture toughness measured using sharply-notched samples instead of pre-fatigue-cracked ones can give a reasonable (albeit slightly inflated) evaluation of the damage tolerance of the Ti-rich multiphase composite. However, the mechanical properties of BMGs and BMGCs have been revealed to be much less sensitive to notches compared to their crystalline counterparts [6,26]. As such, notched samples have been widely used to evaluate the fracture toughness of various BMGs and BMGCs [6, 26,27,29,44]. Taking the $\text{Zr}_{39.6}\text{Ti}_{33.9}\text{Nb}_{7.6}\text{Cu}_{6.4}\text{Be}_{12.5}$ (DH3) BMGCs as an example, the notched fracture toughness is comparable to that obtained using pre-fatigue-cracked samples [28,29].

Additionally, the current composite is distinguished from most of other BMGCs by its large uniform deformation under both tensile and flexural loading conditions. Uniform elongations over 1% are rarely attainable in the MG-matrix composites fabricated by *ex situ* methods [17–19]; in general, it is also quite limited in most of *in situ* BMGCs except for those toughened by the B2–CuZr phase which undergoes martensitic transformation induced plasticity [8,12–14,16]. To date, comparably good combinations of high values of strength, fracture toughness and uniform elongation have only been obtained in Ti/Zr-based BMGCs which tend to exhibit larger densities than the current composite [8,12–14,16]. Fig. 4(b) provides a comparison between the current composite and BMGCs toughened by *in situ* formed β -type dendrites [8,12–14,16] in terms of fracture toughness and uniform elongation. Although a high toughness can be obtained in the previously reported BMGCs, the uniform elongation can rarely exceed 3% even though the total elongation may exceed 10% (the uniform elongation is markedly lower than the total elongation because of their obvious strain softening behavior). The current composite exhibits a high fracture toughness along with a large uniform elongation of $\sim 4.4\%$, thereby outperforming the BMGCs with uniform composite architectures. Such a good combination of mechanical properties makes the Ti-rich multiphase composite promising for structural applications.

4. Conclusions

In summary, a Ti-rich multiphase composite with hierarchical architecture was processed from metallic glasses (MGs) and pure Ti alloys by precise tailoring of the structural heterogeneity. The Ti-rich multiphase composite, which consists of MG, α -Ti and β -Ti phases, exhibits a relatively low density of $4.95 \text{ g} \cdot \text{cm}^{-3}$ due to its high Ti content of 66.4 at.%. The Ti layers in the Ti-rich multiphase composite become thinner to form β -Ti dendrites and lead to zig-zag interfaces between MG and Ti layers because of the liquid/solid interaction encompassing atomic diffusion. Additionally, the α -Ti layer exhibits a gradient nature with varying content of elements and increasing grain size from the exterior to interior regions. Such a heterogeneous architecture endows the Ti-rich multiphase composite with an outstanding combination of mechanical properties, including a high ultimate tensile strength of $\sim 1408 \text{ MPa}$, tensile elongation of $\sim 7.1\%$, flexural strength of $\sim 2714 \text{ MPa}$, and

flexural plasticity of $\sim 10.3\%$. Additionally, the architecture acts to promote shear band multiplication, crack blunting and crack deflection, and to create constrained microcracking ahead of the crack tip as an inelastic deformation mechanism to resist fracture; these mechanisms act *in concert* to result in a high fracture toughness of $\sim 109 \text{ MPa} \cdot \text{m}^{1/2}$. In contrast, the reference *in situ* homogeneous BMGC, which has a similar composition but displays a uniform composite architecture, exhibits much poorer mechanical properties. The uniform architecture cannot effectively inhibit the propagation of shear bands in the MG phase or resist crack extension, leading to limited fracture toughness that is 61% lower than that of the Ti-rich multiphase composite. This study is intended to provide useful insights for the architectural design and construction of high-strength composite materials with enhanced damage tolerance, and may increase their potential for critical structural applications.

Author contributions

S.F.L. and Z.W.Z. initiated this project and designed the experiments. S.F.L., S.F.G., D.M.L, H.L. and Z.K.L. synthesized the samples. S.F.L, D.M. L., H.M.F. and A.M.W characterized the samples and performed the properties measurements. S.F.L., Z.W.Z, Z.Q.L., Z.F.Z, Z.H.Z. and R.O.R. analyzed the data. S.F.L. and Z.W.Z. wrote the original manuscript, Z.W. Z., Z.Q.L. and R.O.R. supervised the research and revised the manuscript. All the authors discussed the results.

Declaration of competing interest

The authors declare that they have no known competing financial interests or personal relationships that could have appeared to influence the work reported in this paper.

Data availability

Data will be made available on request.

Acknowledgements

ZWZ is grateful for the financial support by the National Natural Science Foundation of China under grant number 52074257 and Chinese Academy of Sciences. ZL is grateful for the financial support by the National Key R&D Program of China under grant number 2020YFA0710404, the National Natural Science Foundation of China under grant numbers 52173269 and 51871216, the KC Wong Education Foundation (GJTD-2020-09), and the Youth Innovation Promotion Association CAS. Support for R.O.R. was provided by the US Air Force Office of Scientific Research, under the MURI grant AFSOR-FA9550-15-1-0009.

Appendix A. Supplementary data

Supplementary data to this article can be found online at <https://doi.org/10.1016/j.compositesb.2023.110818>.

References

- [1] Trang TTT, Zhang JH, Kim JH, Zargaran A, Hwang JH, Suh BC, Kim NJ. Designing a Magnesium alloy with high strength and high formability. *Nat Commun* 2018;9: 2522.
- [2] Liddicoat PV, Liao XZ, Zhao Y, Zhu Y, Murashkin MY, Lavernia EJ, Valiev RZ, Ringer SP. Nanostructural hierarchy increases the strength of aluminium alloys. *Nat Commun* 2010;1:63.
- [3] Pu B, Zhang X, Chen X, Lin X, Zhao D, Shi C, Liu E, Sha J, He C, Zhao N. Exceptional mechanical properties of aluminum matrix composites with heterogeneous structure induced by in-situ graphene nanosheet-Cu hybrids. *Compos B Eng* 2022; 234:109731.
- [4] Greer AL, Cheng YQ, Ma E. Shear bands in metallic glasses. *Mater Sci Eng, A R* 2013;74:71–132.

- [5] Qiao J, Jia H, Liaw PK. Metallic glass matrix composites. *Mater Sci Eng, A R* 2016; 100:1–69.
- [6] Gu XJ, Poon SJ, Shiflet GJ, Lewandowski JJ. Compressive plasticity and toughness of a Ti-based bulk metallic glass. *Acta Mater* 2010;58:1708–20.
- [7] Tang MQ, Zhang HF, Zhu ZW, Fu HM, Wang AM, Li H, Hu ZQ. TiZr-base bulk metallic glass with over 50 mm in diameter. *J Mater Sci Technol* 2010;26:481–6.
- [8] Hofmann DC, Suh JY, Wiest A, Lind ML, Demetriou MD, Johnson WL. Development of tough, low-density Titanium-based bulk metallic glass matrix composites with tensile ductility. *Proc Natl Acad Sci USA* 2008;105:20136–40.
- [9] Guo H, Yan PF, Wang YB, Tan J, Zhang ZF, Sui ML, Ma E. Tensile ductility and necking of metallic glass. *Nat Mater* 2007;6:735–9.
- [10] Demetriou MD, Launey ME, Garrett G, Schramm JP, Hofmann DC, Johnson WL, Ritchie RO. A damage-tolerant glass. *Nat Mater* 2011;10:123–8.
- [11] Lewandowski JJ, Greer AL. Temperature rise at shear bands in metallic glasses. *Nat Mater* 2005;5:15–8.
- [12] Hofmann DC, Suh JY, Wiest A, Duan G, Lind ML, Demetriou MD, Johnson WL. Designing metallic glass matrix composites with high toughness and tensile ductility. *Nature* 2008;451:1085–9.
- [13] Narayan RL, Singh PS, Hofmann DC, Hutchinson N, Flores KM, Ramamurty U. On the microstructure - tensile property correlations in bulk metallic glass matrix composites with crystalline dendrites. *Acta Mater* 2012;60:5089–100.
- [14] Oh YS, Kim CP, Lee S, Kim NJ. Microstructure and tensile properties of high-strength high-ductility Ti-based amorphous matrix composites containing ductile dendrites. *Acta Mater* 2011;59:7277–86.
- [15] Wu Y, Xiao Y, Chen G, Liu CT, Lu Z. Bulk metallic glass composites with transformation-mediated work-hardening and ductility. *Adv Mater* 2010;22: 2770–3.
- [16] Liu D, Zhu Z, Li Z, Zhang L, Fu H, Wang A, Li H, Zhang H, Wang Y, Zhang H. Modulating work-hardening behaviors and tensile plasticity of in-situ formed ductile dendrite Ti-based bulk metallic glass composites with tailored dendrite composition. *Scripta Mater* 2018;146:22–6.
- [17] Gao WJ, Zhang WW, Zhang T, Yang C, Huang XS, Liu ZY, Wang Z, Li WH, Li WR, Li L, Liu LH. Large tensile plasticity in Zr-based metallic glass/stainless steel interpenetrating-phase composites prepared by high pressure die casting. *Compos B Eng* 2021;224:109226.
- [18] Wat A, Lee JI, Ryu CW, Gludovatz B, Kim J, Tomsia AP, Ishikawa T, Schmitz J, Meyer A, Alfreider M, Kiener D, Park ES, Ritchie RO. Bioinspired nacre-like alumina with a bulk-metallic glass-forming alloy as a compliant phase. *Nat Commun* 2019;10:961.
- [19] Chen S, Li WQ, Zhang L, Fu HM, Li ZK, Zhu ZW, Li H, Zhang HW, Wang AM, Wang YD, Zhang HF. Dynamic compressive mechanical properties of the spiral tungsten wire reinforced Zr-based bulk metallic glass composites. *Compos B Eng* 2020;199:108219.
- [20] Wang M, Huang MX. Abnormal TRIP effect on the work hardening behavior of a quenching and partitioning steel at high strain rate. *Acta Mater* 2020;188:551–9.
- [21] Ellyson B, Klemm-Toole J, Clarke K, Field R, Kaufman M, Clarke A. Tuning the strength and ductility balance of a TRIP titanium alloy. *Scripta Mater* 2021;194: 113641.
- [22] Su J, Jiang F, Tan C, Weng F, Ng FL, Goh MH, Xie H, Liu J, Chew Y, Teng J. Additive manufacturing of fine-grained high-strength titanium alloy via multi-eutectoid elements alloying. *Compos B Eng* 2023;249:110399.
- [23] Zhang L, Su S, Fu W, Sun J, Ning Z, Ngan AHW, Huang Y. Strain-induced structural evolution of interphase interfaces in CuZr-based metallic-glass composite reinforced by B2 crystalline phase. *Compos B Eng* 2023;258:110698.
- [24] Liu DM, Lin SF, Zhu ZW, Zhang B, Li ZK, Zhang L, Fu HM, Wang AM, Li H, Zhang HW, Zhang HF. The design and mechanical behaviors of in-situ formed ductile dendrite Ti-based bulk metallic glass composites with tailored composition and mechanisms. *Mater Sci Eng A* 2018;732:148–56.
- [25] He Q, Shang JK, Ma E, Xu J. Crack-resistance curve of a Zr-Ti-Cu-Al bulk metallic glass with extraordinary fracture toughness. *Acta Mater* 2012;60:4940–9.
- [26] He Q, Cheng YQ, Ma E, Xu J. Locating bulk metallic glasses with high fracture toughness: chemical effects and composition optimization. *Acta Mater* 2011;59: 202–15.
- [27] Chen W, Ketkaew J, Liu Z, Mota RMO, O'Brien K, da Silva CS, Schroers J. Does the fracture toughness of bulk metallic glasses scatter? *Scripta Mater* 2015;107:1–4.
- [28] Launey ME, Hofmann DC, Suh J-Y, Kozachkov H, Johnson WL, Ritchie RO. Fracture toughness and crack-resistance curve behavior in metallic glass-matrix composites. *Appl Phys Lett* 2009;94:241910.
- [29] Rajpoot D, Narayan RL, Zhang L, Kumar P, Zhang H, Tandaiya P, Ramamurty U. Shear fracture in bulk metallic glass composites. *Acta Mater* 2021;213:116963.
- [30] Barthelat F, Tang H, Zavattieri P, Li CM, Espinosa H. On the mechanics of mother-of-pearl: a key feature in the material hierarchical structure. *J Mech Phys Solid* 2007;55:306–37.
- [31] Meyers MA, McKittrick J, Chen PY. Structural biological materials: critical mechanics-materials connections. *Science* 2013;339:773–9.
- [32] Wegst UG, Bai H, Saiz E, Tomsia AP, Ritchie RO. Bioinspired structural materials. *Nat Mater* 2015;14:23–36.
- [33] Amini A, Khavari A, Barthelat F, Ehrlicher AJ. Centrifugation and index matching yield a strong and transparent bioinspired nacreous composite. *Science* 2021;373: 1229–34.
- [34] Zhang M, Zhao N, Yu Q, Liu Z, Qu R, Zhang J, Li S, Ren D, Berto F, Zhang Z. On the damage tolerance of 3-D printed Mg-Ti interpenetrating-phase composites with bioinspired architectures. *Nat Commun* 2022;13:1–13.
- [35] Munch E, Launey ME, Alsem DH, Saiz E, Tomsia AP, Ritchie RO. Tough, bio-inspired hybrid materials. *Science* 2008;322:1516–20.
- [36] Li PY, Li XN, Liu ZY, Chen LQ, Xiao BL, Ma ZY. Enhanced strength–ductility synergy of carbon nanotube/Al–Cu–Mg composites via introducing laminate structure and grain modification. *Compos B Eng* 2022;243:110178.
- [37] Takeuchi A, Inoue A. Classification of bulk metallic glasses by atomic size difference, heat of mixing and period of constituent elements and its application to characterization of the main alloying element. *Mater Trans* 2005;46:2817–29.
- [38] Wu XL, Jiang P, Chen L, Zhang JF, Yuan FP, Zhu YT. Synergetic strengthening by gradient structure. *Mater Res Lett* 2014;2:185–91.
- [39] Liu Z, Meyers MA, Zhang Z, Ritchie RO. Functional gradients and heterogeneities in biological materials: design principles, functions, and bioinspired applications. *Prog Mater Sci* 2017;88:467–98.
- [40] Alabort E, Barba D, Shagiev MR, Murzinova MA, Galeyev RM, Valiakhmetov OR, Aletdinov AF, Reed RC. Alloys-by-design: application to titanium alloys for optimal superplasticity. *Acta Mater* 2019;178:275–87.
- [41] Kim WS, Yun IH, Lee JJ, Jung HT. Evaluation of mechanical interlock effect on adhesion strength of polymer–metal interfaces using micro-patterned surface topography. *Int J Adhesion Adhes* 2010;30:408–17.
- [42] Liu Z, Zhang Z, Ritchie RO. Interfacial toughening effect of suture structures. *Acta Biomater* 2020;102:75–82.
- [43] Zhou X, Chen C. Strengthening and toughening mechanisms of amorphous/amorphous nanolaminates. *Int J Plast* 2016;80:75–85.
- [44] Gu XJ, Poon SJ, Shiflet GJ, Lewandowski JJ. Ductile-to-brittle transition in a Ti-based bulk metallic glass. *Scripta Mater* 2009;60:1027–30.
- [45] Cao R, Yu Q, Pan J, Lin Y, Sweet A, Li Y, Ritchie RO. On the exceptional damage-tolerance of gradient metallic materials. *Mater Today* 2020;32:94–107.
- [46] Sun Y, Chen J, Ma F, Ameyama K, Xiao W, Ma C. Tensile and flexural properties of multilayered metal/intermetallics composites. *Mater Char* 2015;102:165–72.
- [47] Ren L, Xiao W, Chang H, Zhao Y, Ma C, Zhou L. Microstructural tailoring and mechanical properties of a multi-alloyed near β titanium alloy Ti-5321 with various heat treatment. *Mater Sci Eng A* 2018;711:553–61.
- [48] Wang H, Zhao Q, Xin S, Zhao Y, Zhou W, Zeng W. Microstructural morphology effects on fracture toughness and crack growth behaviors in a high strength titanium alloy. *Mater Sci Eng A* 2021;821:141626.
- [49] Nyakana SL, Fanning JC, Boyer RR. Quick reference guide for β Titanium alloys in the 00s. *J Mater Eng Perform* 2005;14:799–811.
- [50] Xu J, Zeng W, Zhou D, Ma H, Chen W, He S. Influence of alpha/beta processing on fracture toughness for a two-phase titanium alloy. *Mater Sci Eng A* 2018;731: 85–92.
- [51] Bhattacharjee A, Varma VK, Kamat SV, Gogia AK, Bhargava S. Influence of β grain size on tensile behavior and ductile fracture toughness of Titanium alloy Ti-10V-2Fe-3Al. *Metall Mater Trans A* 2006;37:1423–33.
- [52] Chen F, Gu Y, Xu G, Cui Y, Chang H, Zhou L. Improved fracture toughness by microalloying of Fe in Ti-6Al-4V. *Mater Des* 2020;185:108251.
- [53] Semenova IP, Modina JM, Polyakov AV, Klevtsov GV, Klevtsova NA, Pigaleva IN, Valiev RZ, Langdon TG. Fracture toughness at cryogenic temperatures of ultrafine-grained Ti-6Al-4V alloy processed by ECAP. *Mater Sci Eng A* 2018;716:260–7.
- [54] Kumar P, Ramamurty U. Microstructural optimization through heat treatment for enhancing the fracture toughness and fatigue crack growth resistance of selective laser melted Ti-6Al-4V alloy. *Acta Mater* 2019;169:45–59.
- [55] Yu Y, Hui S, Ye W, Xiong B. Mechanical properties and microstructure of an $\alpha + \beta$ titanium alloy with high strength and fracture toughness. *Rare Met* 2009;28:346–9.
- [56] Manikandan P, Kumar KN, Rao GS, Jha AK, Narayanan PR, Pant B, Cherian RM. Fracture toughness of Ti-15V-3Cr-3Sn-3Al Titanium alloy in different heat-treated conditions. *Trans Indian Inst Met* 2019;72:1507–10.
- [57] Peng X, Guo H, Wang T, Yao Z. Effects of β treatments on microstructures and mechanical properties of TC4-DT titanium alloy. *Mater Sci Eng A* 2012;533:55–63.
- [58] Guo P, Zhao Y, Zeng W, Hong Q. The effect of microstructure on the mechanical properties of TC4-DT titanium alloys. *Mater Sci Eng A* 2013;563:106–11.
- [59] Wen X, Wan M, Huang C, Tan Y, Lei M, Liang Y, Cai X. Effect of microstructure on tensile properties, impact toughness and fracture toughness of TC21 alloy. *Mater Des* 2019;180:107898.
- [60] Shi ZF, Guo HZ, Han JY, Yao ZK. Microstructure and mechanical properties of TC21 titanium alloy after heat treatment. *Trans Nonferrous Met Soc China* 2013; 23:2882–9.
- [61] Zhao YQ, Qu HL, Chen J. Research on Titanium alloys with high toughness and high damage tolerance. *Mater Sci Forum* 2009;618–619:97–100.
- [62] Liu Y, Lim SCV, Ding C, Huang A, Weyland M. Unravelling the competitive effect of microstructural features on the fracture toughness and tensile properties of near β titanium alloys. *J Mater Sci Technol* 2022;97:101–12.
- [63] Wu C, Zhan M. Microstructural evolution, mechanical properties and fracture toughness of near β Titanium alloy during different solution plus aging heat treatments. *J Alloys Compd* 2019;805:1144–60.
- [64] Fan JK, Li JS, Kou HC, Hua K, Tang B. The interrelationship of fracture toughness and microstructure in a new near β Titanium alloy Ti-7Mo-3Nb-3Cr-3Al. *Mater Char* 2014;96:93–9.
- [65] Sabirov I, Valiev RZ, Semenova IP, Pippan R. Effect of equal channel angular pressing on the fracture behavior of commercially pure Titanium. *Metall Mater Trans A* 2010;41:727–33.